

# An Idea of Implementing Photonic Space-Time Crystals Using Metasurfaces

ONTA SHAHRIAR AND M.R.C. MAHDY\*

*Department of Electrical and Computer Engineering, North South University, Bashundhara, Dhaka-1229, Bangladesh*

*\*[mahdy.chowdhury@northsouth.edu](mailto:mahdy.chowdhury@northsouth.edu)*

**Abstract:** Photonic space-time crystals (PSTCs) are emerging materials characterized by periodic variations in electromagnetic parameters with respect to both space and time. To date, research on PSTCs remains theoretical, with no practical realization reported. This article presents the practical realization of PSTCs through the design and simulation of a 2D metasurface-based photonic space-time crystal. It illustrates the characteristics of energy bandgaps, momentum bandgaps, and mixed energy–momentum bandgap eigenmodes within the dispersion relation of these crystals. Additionally, the article details the properties of second-order exceptional points that occur when two bandgaps overlap under specific conditions. The application of the metasurface-based PSTC in 6G wireless communications is also demonstrated. This work aims to advance the understanding of PSTCs and their potential applications.

metasurfaces, space-time crystals, mixed energy-momentum bandgaps, exceptional points

## 1. Introduction

Photonic time crystals (PTCs) are materials whose electromagnetic parameters, such as permittivity, refractive index, etc., vary periodically with respect to time with large amplitude and high frequency, thereby exhibiting momentum bandgaps. The study of wave propagation through time-varying media began in the 1950s [1–5]. When an electromagnetic (EM) wave propagates through a PTC with a modulation frequency comparable to the EM wave's frequency, it experiences time reflection and time refraction [3, 5, 6]. This process results in two new waves with wavenumbers of opposite polarity: a time-refracted wave propagating in the same direction, and a time-reflected wave propagating in the direction opposite to the original wave due to causality constraints preventing backward time propagation. In PTCs, where electromagnetic parameters vary periodically throughout the bulk media, momentum ( $\mathbf{P}$ ) is conserved, resulting in the same wavenumber ( $\mathbf{K}$ ) for the resulting waves as the initial wave, because in electromagnetism, the momentum of the wave is,  $\mathbf{P} = \hbar\mathbf{K}$ . However, energy is not conserved, leading to refracted and reflected waves having different frequencies from the original wave. Periodic modulation of electromagnetic properties creates multiple time-reflected and time-refracted waves, which interfere with each other to form a PTC [2, 5, 7, 8]. This interference generates a dispersion relation for PTCs where Floquet eigenmodes are organized into a band structure with bands and bandgaps along the momentum axis. The eigenvalues of the Floquet modes  $\Omega_f$  (quasi-energies) are real within the bands and complex within the momentum bandgaps. Within momentum bandgaps, the modulation of PTC's parameters can lead to exponential growth and decay of wave amplitude simultaneously, although ultimately the growth dominates. This exponentially amplifying feature of momentum bandgaps has numerous applications. Within momentum bandgaps, waves with wavenumbers falling within the bandgap range are exponentially amplified, with amplification decreasing closer to the bandgap boundaries. The formation of momentum bandgaps primarily depends on the amplitude and frequency of modulation of the PTC, influencing the breadth and height of the momentum bandgaps. Momentum bandgaps are created only when the amplitude and frequency of modulation are high. If these conditions are not satisfied, the time-reflected waves

created by wave propagation through the PTC will be of low intensity, and the dispersion relation will not exhibit a wide and tall momentum bandgap. These conditions distinguish PTCs fundamentally from optical parametric amplifiers (OPAs), which operate on resonance. PTCs can be considered temporal counterparts of Photonic Crystals (PCs), where electromagnetic parameters vary periodically with respect to space instead of time. Despite their similarity in type, there are major differences between them: PTCs break time-translation symmetry and conserve momentum, whereas dielectric PCs break spatial-translation symmetry and conserve energy. For these reasons, the wavenumber is the preferred quantum number for analyzing PTCs, with the band structure constructed along the wavenumber axis on the dispersion relation showing momentum bands and bandgaps along that axis. PCs, on the other hand, use energy as the quantum number, depicting energy bands and bandgaps along the dispersion relation's energy axis.

Another important distinction between PTCs and PCs lies in the characteristics of the eigenmodes within the bands and bandgaps. In PCs, eigenmodes within the energy bandgap exhibit exponentially decaying amplitudes due to energy conservation, which restricts growth in the energy of resulting waves. Conversely, eigenmodes within the bandgaps of PTCs exhibit both exponentially growing and decaying amplitudes, extracting energy from the modulating source. Recognizing the useful features of PTCs, researchers have heavily studied them, uncovering aspects such as momentum bandgaps [9], topological aspects [10], parity-time symmetry [11], temporal aiming [12], localization via temporal disorder [13], and others [14–18]. To practically realize PTCs that can work with electromagnetic waves having high frequencies, materials are needed whose electromagnetic parameters can be periodically modulated with large amplitude and high frequency, yet such materials currently do not exist. The potential for PTCs to function in the sub-terahertz and optical frequency ranges depends on epsilon-near-zero materials (ENZ) [19–23] currently under research, whose refractive index can be modulated with an amplitude around 1 and a frequency in the petahertz range. The modulation of a material's properties at low frequencies can be achieved using electronic components like varactors, as demonstrated by observing momentum bandgaps at microwave frequencies [8].

To date, only theoretical research has been conducted on Photonic Space-Time Crystals (PSTCs), and practical realization remains elusive. Modulating a material's properties practically with respect to time at low frequencies can be accomplished using electronic components such as varactors. However, implementing a large 3D network of electronic components for a 3D material is highly complex and challenging. Moreover, the electrical signals in the network's wires may emit electromagnetic waves that interfere with propagating EM waves. At optical frequencies, temporal modulation of a 3D bulk media can be achieved using laser pumping, which generates and depletes ultrafast free electrons. However, due to the focused nature of lasers, achieving uniform modulation of a material's properties throughout the bulk media is impractical. Nonetheless, modulation of a 2D surface's properties at microwave frequencies using electronic components is feasible and can be practically realized.

Space-time-modulated metasurface structures have already been used for frequency conversion [24] and non-reciprocal frequency generation [25]. However, to the best of our knowledge, the implementation of PSTC using metasurfaces has not yet been achieved. In this article, we demonstrate our practical realization of a PSTC by designing and simulating a 2D metasurface-based photonic space-time crystal. We explore the different eigenmodes provided by the dispersion relation of a PSTC, studying how Transverse Electric (TE) waves excite various

eigenmodes while propagating along the 2D metasurface-based PSTC. PSTCs are materials whose electromagnetic parameters are periodically modulated in both time and space. We observe that the band structure of such PSTCs contains energy bandgaps, momentum bandgaps due to periodic modulation in time, and novel mixed momentum–energy bandgaps. The intriguing mixed momentum–energy bandgap is unique to PSTCs, formed by applying a modulation frequency that causes a momentum bandgap and an energy bandgap to partially overlap. The eigenmodes in these bandgaps attain both a complex Bloch wavenumber  $K_B$  and a complex Floquet frequency  $\Omega_f$ , exhibiting coupling of energy to eigenmodes with complex quasi-energy and momentum. In the mixed momentum–energy bandgaps, the ratio between the imaginary values of the Bloch wavenumber  $K_B$  and the Floquet frequency  $\Omega_f$  determines the characteristics of the eigenmodes inside the mixed momentum–energy bandgap. Depending on the ratio of  $\text{Im}(\Omega_f)$  and  $\text{Im}(K_B)$ , these mixed bandgaps can host different types of eigenmodes. Some mixed bandgap eigenmodes correspond to the localization of EM waves while maintaining approximately the same energy; others lead to exponential growth of EM amplitude, and some result in linear power growth of the EM wave. We found that the size of the mixed momentum–energy bandgap depends on the overlap between the energy and momentum bandgaps, and it shrinks as the overlap increases. Under very strict conditions, both the energy and momentum bandgaps superimpose onto each other, causing the mixed energy–momentum bandgap to collapse to a 2nd-order exceptional point, which corresponds to an eigenmode exhibiting linear power growth. Due to the wide range of intriguing features of PSTCs, it has become important to start practically realizing PSTCs to facilitate more research and discover novel features. For this purpose, in this paper, we propose a metasurface-based Photonic Space-Time Crystal (PSTC). Lastly, we also demonstrate how our proposed metasurface-based Photonic Space-Time Crystal (PSTC) can be used as a surface antenna for 6G wireless communications.

## 2. Unit cell structure and dispersion relation of the 2D photonic space-time crystal

We used the metasurface structure shown in Fig. 1(b) to create the metasurface-based PSTC. The unit cell designed for constructing the complete metasurface is depicted in Fig. 1(a). All dimensions of the unit cell are labeled in Fig. 1(a), and their values are provided in the figure description. The metasurface shown in Fig. 1(b) is composed by assembling 9 such unit cells along the x-axis. The structure and operational principles are detailed in Supplemental 1 of this paper (S2 and S3). At the bottom, there is a Flame-Retardant Glass-Reinforced Epoxy Laminate material (FR-4) substrate measuring 90 mm in length, 40 mm in width, and 0.9 mm in height. Above it, there is a grounded copper layer with the same dimensions as the FR-4 substrate but with a height of 0.1 mm. This copper layer includes a 2 mm radius hole, visible in Fig. 1(a) in order to keep one of the two vias ungrounded. Placed atop this copper layer is another FR-4 block measuring 50 mm in length, 40 mm in width, and 2.4 mm in height. On top of this block are two copper plates, each 0.1 mm thick and separated by a 1 mm gap. To connect the circuit components beneath the FR-4 substrate with the two top copper plates and the grounded copper plate, two vias with a radius of 1 mm are used. Two perfect electric conductor (PEC) blocks are positioned on the outer sides of the FR-4 block and the two copper plates for electromagnetic shielding. At the very bottom, 2 mm wide and 0.1 mm thick copper tracks are used as wires. These wires connect the 2.2  $\mu\text{F}$  capacitor and the diode to their respective vias. An L-shaped wire is employed to connect the common node between the capacitor and diode for feeding the modulation signal. Additionally, a DC voltage and inductor connected in series are linked to the common node. All copper plates utilized in the structure have a thickness of 0.1 mm. The grey-colored blocks in Fig. 1(b) are made of perfect electric conductor (PEC) material. Here, we used lossy FR-4 with  $\epsilon = 4.3$  F/m,  $\mu = 1$  H/m, and  $\tan \delta = 0.025$ . The surface

capacitance of the metasurface varies according to a coordinate-separable space and time-dependent function, as shown below:

$$C(t, x) = C_0 \times C(t) \times C(x) \quad (1)$$

Here,  $C_0$  is the intrinsic surface capacitance of the unit cells used in our metasurface and is equal to 1 pF. The functions  $C(t)$  and  $C(x)$  are periodic in time and space, respectively, so they together create a space- and time-varying crystal. The equation of our 2D space-time crystal with a modulation frequency of 0.75 GHz and spatial period of 160 mm is given here:

$$C(t, x) = C_0 \times (1 + (0.3 \times \cos(4.71 \times t))) \times (1 + (0.3 \times \cos(0.04 \times x))) \quad (2)$$

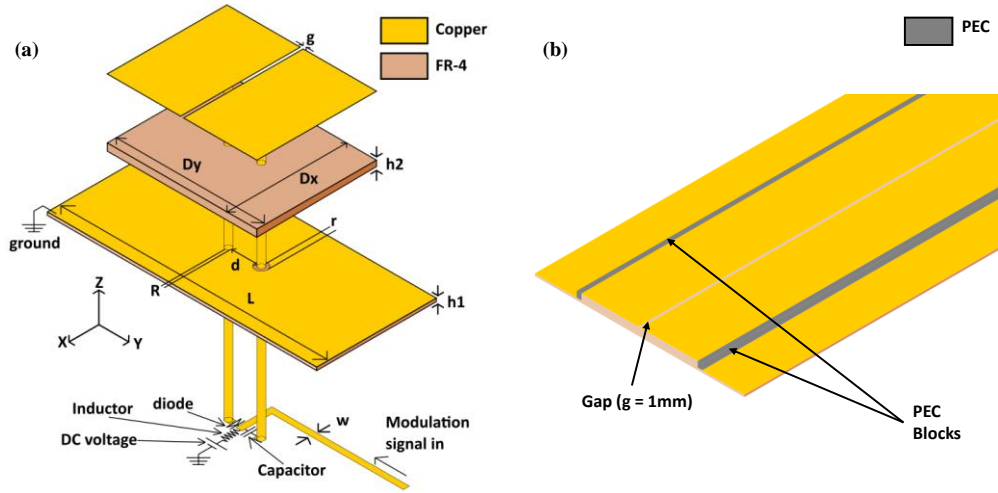


**Fig. 1.** (a) Exploded isometric view of the unit cell structure of the metasurface.  $g = 1\text{mm}$ ,  $D_y = 50\text{mm}$ ,  $D_x = 40\text{mm}$ ,  $h_2 = 2.4\text{mm}$ ,  $h_1 = 1\text{mm}$ ,  $r = 2\text{mm}$ ,  $R = 1\text{mm}$ ,  $L = 90\text{mm}$ ,  $w = 2\text{mm}$ ,  $d = 9\text{mm}$ . (b) A part of the complete metasurface structure is created by joining 9 unit cells along the x-axis.

The 3D figure of Eq. (2) is depicted in Fig. 2(a). Here, we used eigenvalue approach to find the eigenmodes. Eigenvalue approach is not only applicable to bulk media systems, it is also applicable to metasurface structures. Here, the transverse electric surface waves propagate through the free space over the metasurface. Moreover, the modulation of surface capacitance creates alternating electric fields between the two top copper plates and these fields stay within the bulk free space above the metasurface. So, as both transverse electric surface waves and the alternating electric fields due to changing surface capacitance stay within the bulk free space over the metasurface, eigenvalue approach can be used here to find the eigenmodes. We used a coordinate-separable form of the space- and time-varying surface capacitance so that we could easily find the eigenmodes. Due to this coordinate-separable form, the electric field equation can also be written in a coordinate-separable form  $\mathbf{E} = f(t) \times g(x)\mathbf{y}$ . The coordinate-separable form simplifies calculations while still maintaining the functionality of the space-time varying surface capacitance in a non-separable form. The field solution is a product of two different eigenmodes: one is the Floquet mode and the other is the Bloch mode. These eigenmodes can be separately found because we considered a coordinate-separable surface capacitance equation. Subsequently, these eigenmodes are used to form the dispersion relation of the PSTC, shown in Fig. 2(b). The dispersion relation is depicted only up to the first Brillouin zone. The band structure comprises bands and bandgaps. Both Floquet and Bloch eigenmodes

have real and imaginary parts. In band modes, both Floquet and Bloch modes have zero imaginary parts and only real parts. In energy bandgap mode, only Bloch modes have nonzero imaginary parts and a constant real part equal to 1. In momentum bandgap mode, only Floquet modes have nonzero imaginary parts and a constant real part equal to 1, as shown in Fig. 2(b). Now, the calculation of eigenvalues is shown below:

$$\Rightarrow \nabla \times \nabla \times \mathbf{E} = \nabla \times \left( -\frac{\delta}{\delta t} \mathbf{B} \right) = -\mu_0 \times \frac{\delta}{\delta t} (\nabla \times \mathbf{H}) \quad (3)$$

Using the Ampère-Maxwell law in differential form, along with the coordinate-separable form of surface capacitance, Eq. (1), and the displacement current equation derived in Supplemental 1 (S1), we obtain:

$$\begin{aligned} &= -\mu_0 \times C_0 \times g(x) \times C(x) \times \frac{d^2}{dt^2} (f(t) \times C(t)) \mathbf{y} \\ &= -\mu_0 \times C_0 \times g(x) \times C(x) \times ((f(\ddot{t}) \times C(t)) + (2 \times C(\dot{t}) \times f(\dot{t})) + (C(\ddot{t}) \times f(t))) \mathbf{y} \quad (4) \end{aligned}$$

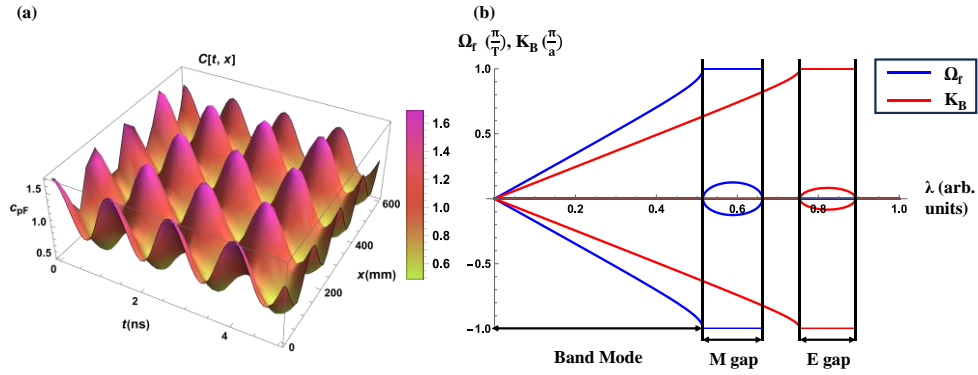


**Fig. 2.** (a) Space- and time-varying surface capacitance of the metasurface. Here, our 2D PSTC crystal has a spatial period of 160 mm and a modulation frequency of 0.75 GHz. (b) The band structure of the 2D photonic space-time crystal with a spatial period of 160 mm and a modulation frequency of 0.75 GHz. The blue curve represents the complex value of Floquet frequency ( $\Omega_f$ ), and the red curve represents the complex value of Bloch wavenumber ( $K_B$ ).

The blue ellipse represents the imaginary part of  $\Omega_f$  and the red ellipse represents the imaginary part of  $K_B$ . In momentum bandgap (M gap),  $\Omega_f$  has a constant real part and nonzero imaginary part. In the energy bandgap (E gap),  $K_B$  has a constant real part and nonzero imaginary part. In the Band mode, both  $K_B$  and  $\Omega_f$  have only real parts and no imaginary parts.  $\lambda$  is a unitless parameter used here for solving the coordinate-separable differential equation, Eq. (6).

Moreover, we know that,

$$\begin{aligned} \Rightarrow \nabla \times \nabla \times \mathbf{E} &= \nabla \cdot \nabla \cdot \mathbf{E} - \nabla^2 \mathbf{E} \\ &= -\nabla^2 (f(t) \times g(x)) \mathbf{y} \quad (5) \end{aligned}$$

Equating Eq. (5) and Eq. (4), we get the following coordinate separable differential equation:

$$\begin{aligned} \Rightarrow \frac{\frac{d^2}{dx^2} g(x)}{C(x) \times g(x)} &= \frac{((f(\ddot{t}) \times C(t)) + (2 \times C(\dot{t}) \times f(\dot{t})) + (C(\ddot{t}) \times f(t)))}{\frac{f(t)}{\mu_0}} \\ &= -\lambda^2 \quad (6) \end{aligned}$$

As can be seen, Eq. (6) has two parts: one is a time-dependent differential equation, and the other part is a space-dependent differential equation. By solving the time-dependent differential equation for values of lambda in the range  $0 \leq \lambda \leq 1$ , we obtain the Floquet modes. By solving the space-dependent differential equation for the value of lambda in the same range  $0 \leq \lambda \leq 1$ , we obtain the Bloch modes. Since both  $C(t)$  and  $C(x)$  are periodic in their respective independent variables, the eigenmodes will take the form of the well-known Bloch wave function, which is commonly used to solve Schrödinger's wave function in periodic potential problems found in condensed matter physics. The electric field equation will be the product of the Bloch and Floquet modes, as shown here,

$$\mathbf{E} = (\exp(ixK_B) \times \exp(it\Omega_f) \times F(x) \times F(t))\mathbf{y} \quad (7)$$

Here,  $K_B$  and  $\Omega_f$  are the characteristic exponents of their respective Bloch wave functions, and  $F(x)$  and  $F(t)$  are the periodic functions of these wave functions. In Eq. (6), lambda ( $\lambda$ ) is a unitless parameter commonly arising when solving coordinate-separable differential equations. In the context of finding Bloch modes, lambda represents angular frequency ( $\omega$ ), while in finding Floquet modes, it represents wavenumber ( $K$ ). By solving the time- and space-dependent differential equations of Eq. (6) for each value of lambda in the range  $0 \leq \lambda \leq 1$ , we obtain the real and imaginary parts of the characteristic exponents  $K_B$  and  $\Omega_f$  in Eq. (7). These are then plotted with respect to lambda to form the dispersion relation shown in Fig. 2(b). From the band structure of the 2D PSTC, we observe three types of eigenmodes. Firstly, there are band modes where both  $K_B$  and  $\Omega_f$  are real with no imaginary parts. Secondly, in the energy bandgap, only  $K_B$  has a nonzero imaginary part and a constant real part equal to 1. Thirdly, in the momentum bandgap, only  $\Omega_f$  has a nonzero imaginary part and a constant real part equal to 1. Under specific conditions, momentum and energy bandgaps may partially overlap, generating unique eigenmodes where both  $K_B$  and  $\Omega_f$  have nonzero imaginary parts and constant real parts equal to 1. These eigenmodes are demonstrated later in this paper. Here, we have used a PSTC of the following form:

$$C(t, x) = C_0 \times (1 + (0.3 \times \cos(\omega \times t))) \times (1 + (0.3 \times \cos(k \times x))) \quad (8)$$

Eq. (8) is a generalized version of Eq. (2), here  $\omega$  and  $k$  are variables. Such a PSTC has multiple energy and momentum bandgaps, but we have plotted the band structure only up to the first Brillouin zone, which contains a single energy and momentum bandgap. The positions of the momentum and energy bandgaps along the  $\lambda$  axis depend on the angular modulation frequency ( $\omega$ ) and spatial wavenumber ( $k$ ) of the PSTC. Therefore, by varying  $\omega$  and  $k$  of the PSTC, we can change the positions of the energy and momentum bandgaps. The unique eigenmodes introduced above, arising due to the partial overlap of momentum and energy bandgaps, can be realized by increasing the modulation frequency of the PSTC from 0.75 GHz to 0.9 GHz. This will cause the two different bandgaps to partially overlap and create new eigenmodes with unique behavior.

### 3. TE wave exciting band, energy bandgap, and momentum bandgap modes

In this section, we studied TE surface wave propagation along the 2D metasurface-based PSTC whose dispersion relation is depicted in Fig. 2(a). In such a crystal, there are three types of eigenmodes: band mode, momentum bandgap mode, and energy bandgap mode. We excited all three types of eigenmodes and observed how the TE surface wave evolved over the 2D PSTC. We used CST Microwave Studio Suite 2021 for performing FDTD simulations of TE surface wave evolution over the 2D PSTC. Initially, we let a TE surface wave propagate along the 2D surface, and at  $t = 5$  ns, we activated the 2D PSTC, which extends over the middle part

of the 2D metasurface. To excite the three types of eigenmodes, we launched TE surface waves with three different frequencies along the metasurface-based PSTC. Figure 2 displays different instances of wave evolution of the TE wave before the PSTC activation and after it was turned on, showing the evolution of the surface wave while propagating over the 2D PSTC. From the simulation results, we found that a TE wave with a frequency of 1.5 GHz can excite the band mode. Exciting a band mode, the TE surface wave couples to the propagating modes, and the surface wave continues to propagate along the metasurface in its initial direction with the same waveform, with slight reflection, as shown in Fig. 3(a) and Fig. 3(b). We also found that a TE wave with a frequency of 1.4 GHz can excite the energy bandgap mode. In the energy bandgap mode, the surface wave stops propagating and remains in the same location over the 2D PSTC while maintaining the same energy. The wave evolution can be seen in Fig. 3(c) and Fig. 3(d). Lastly, we found that a TE wave with a frequency of 3 GHz can excite a momentum bandgap mode. In momentum bandgap mode, once the PSTC is activated, the wave stops propagating, and its amplitude grows exponentially over time due to the imaginary part of the Floquet frequency ( $\Omega_f$ ). Amplified forward and backward wave propagation then takes place along the metasurface. The surface wave evolution can be seen in Fig. 3(e) and Fig. 3(f). The 3 different eigenmodes demonstrated here using the metasurface structure can be applied in photonic integrated circuits (PICs) and silicon photonics as waveguides, amplifiers, and photonic crystals. The band mode can be used as a waveguide in PICs, the momentum bandgap eigenmode can be used as an amplifier in PICs, and the energy bandgap eigenmode can be used as a photonic crystal in PICs.

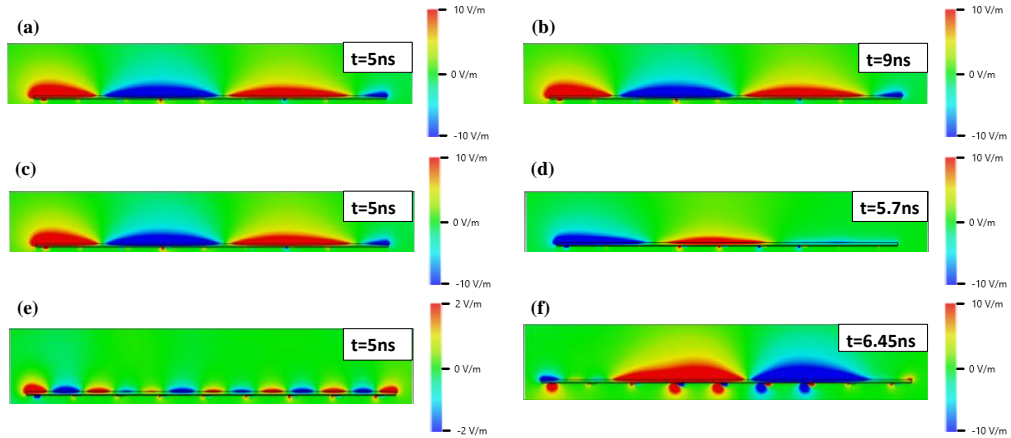


**Fig. 3.** (a) and (b) wave evolution of TE wave exciting band mode. (c) and (d) wave evolution of TE wave exciting energy bandgap mode. (e) and (f) wave evolution of TE wave exciting momentum bandgap mode.

#### 4. TE wave exciting mixed momentum-energy bandgap modes

In this section, we studied mixed momentum-energy bandgap eigenmodes. We found that when we increase the modulation frequency of our PSTC to 0.9 GHz from 0.75 GHz and keep the spatial period at its previous value of 160 nm, the energy and momentum bandgaps partially overlap, as can be seen in Fig. 4. This gives rise to new eigenmodes. The overlapped region is known as the lambda gap, where both Floquet and Bloch modes have nonzero imaginary parts. The lambda gap can be divided into two groups: one where  $\text{Im}(K_B)$  is greater than  $\text{Im}(\Omega_f)$ , and in the other part,  $\text{Im}(\Omega_f)$  is greater than  $\text{Im}(K_B)$ .  $\text{Im}(\Omega_f)$  causes the surface TE wave's amplitude to grow exponentially over time, whereas  $\text{Im}(K_B)$  causes the surface wave's amplitude to decay exponentially over space. In the lambda gap,  $\text{Im}(\Omega_f)$  and  $\text{Im}(K_B)$  oppose each other's effects. If

$\text{Im}(\Omega_f) > \text{Im}(K_B)$ , then the exponential growth of the wave's amplitude in time dominates the nature of the eigenmode, and overall, the eigenmode resembles the momentum bandgap. If  $\text{Im}(\Omega_f) < \text{Im}(K_B)$ , then the exponential decay of the wave's amplitude in space dominates the nature of the eigenmode, and overall, the eigenmode resembles the energy bandgap. We again used CST Microwave Studio Suite 2021 for performing FDTD simulations of the TE surface wave evolution, exciting the two different eigenmodes in the lambda gap. We found that a TE wave with a frequency of 1.4 GHz can excite the mixed energy gap where  $\text{Im}(\Omega_f) < \text{Im}(K_B)$ , and the evolution of the surface wave is shown in Fig. 5(a) and Fig. 5(b). Here, the surface wave stops propagating and becomes localized over the metasurface while maintaining the same energy, as can be seen in Fig. 5(a) and Fig. 5(b). Additionally, we found that a TE surface wave with a frequency of 3 GHz can couple to eigenmodes having  $\text{Im}(\Omega_f) > \text{Im}(K_B)$ . In this case, the surface wave stops propagating, and its amplitude grows exponentially over time, with amplified forward and backward surface waves propagating along the metasurface. The wave evolution is shown in Fig. 5(c) and Fig. 5(d).

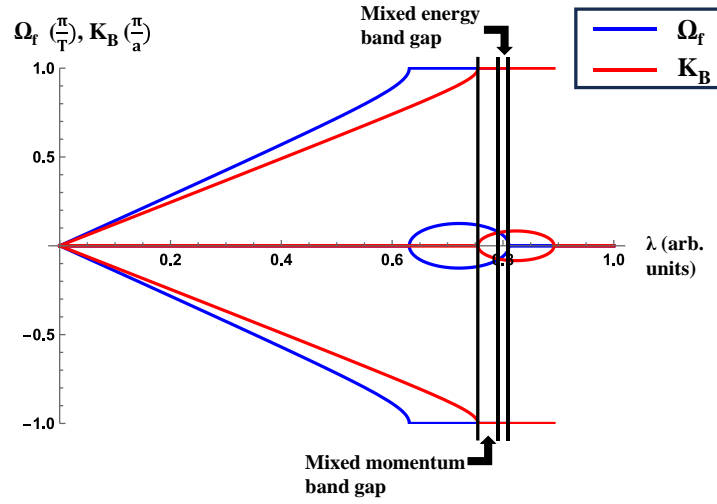


**Fig. 4.** Band structure of a 2D PSTC with partially overlapping bandgaps. In this dispersion relation, there is an energy bandgap, a momentum bandgap, and a lambda gap.

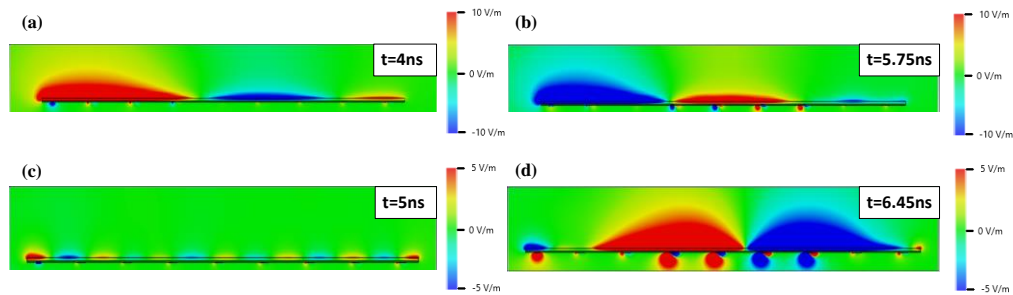


**Fig. 5.** (a) and (b) wave evolution of TE surface wave exciting mixed energy gap mode. The PSTC is activated at  $t = 5\text{ns}$ . (c) and (d) wave evolution of TE surface wave exciting mixed momentum gap mode.



## 5. Exceptional points of a 2D photonic space-time crystal

Finally, we studied a unique case of PSTC where the energy and momentum bandgaps overlap completely, and the imaginary parts of the Floquet and Bloch modes inside the overlapping bandgaps are equal at all values of  $\lambda$  within them. The  $C(t,x)$  function must satisfy two conditions for the perfect overlap of the two bandgaps. Firstly, the modulation period ( $T$ ) of the crystal needed for the complete overlap of the momentum and energy bandgaps should be equal to the following equation:

$$T = \frac{a \times \sqrt{\max(C(t))}}{c} \quad (9)$$

where  $c$  = speed of light in a vacuum in mm/ns,  $a$  is the spatial period in mm, and  $\max(C(t))$  is the maximum value of time-dependent surface capacitance in pF. Here, our PSTC has  $a = 160$ mm and  $\max(C(t)) = 1.3$ pF. Plugging these values into Eq. (9), we get  $T = 0.61$ ns. Then, we calculated the angular modulation frequency ( $\omega$ ) of the PSTC using the Eq. (10) and  $T = 0.61$ ns,

$$\omega = \frac{2 \times \pi}{T} \quad (10)$$

Then, we formed the new  $C(t)$  equation using the new  $\omega$ , and we used the previous  $C(x)$  equation because we did not change the spatial period ( $a$ ). The new equations of  $C(t)$  and  $C(x)$  are given below:

$$C(t) = (1 + (0.3 \times \cos(10.33 \times t))) \quad (11)$$

$$C(x) = (1 + (0.3 \times \cos(0.04 \times x))) \quad (12)$$

For  $0 \leq x \leq a$  and  $0 \leq t \leq T$ , where  $a = 160$ mm and  $T = 0.61$ ns, let

$$\beta = \frac{x}{a} = \frac{t}{T}; 0 \leq \beta \leq 1 \quad (13)$$

The product of the time-dependent surface capacitance equation, Eq. (11), and the space-dependent surface capacitance equation, Eq. (12), at any value of  $\beta$ , has to be equal to a real positive constant number ( $L$ ).

$$C_t(\beta) \times C_x(\beta) = L \quad (14)$$

This is the second condition, and we found that our crystal, with  $a = 160$  mm and  $T = 0.61$  ns, satisfies this condition with  $L = 1.69$  for any value of  $\beta$  in the range  $0 \leq \beta \leq 1$ . It is known that the edges of both the energy bandgap and momentum bandgap consist of exceptional points [26]. Exceptional points are formed by the coalescence of eigenvalues and their corresponding eigenvectors. Similarly, in our case, the bandgap edges in the dispersion relation of the PSTC also contain exceptional points. Therefore, when the energy and momentum bandgaps overlap perfectly, the exceptional points and corresponding eigenvalues also overlap, forming 2nd-order exceptional points. This overlapping of exceptional points to form higher-order exceptional points is unique to this system and produces eigenmodes with unique behavior. Here, we simulated the evolution of a TE surface wave coupling to the 2nd-order exceptional point. When we set the modulation frequency of the PSTC to 1.64 GHz, we found that our 2D PSTC has the dispersion relation shown in Fig. 6. We observed that a TE surface wave with a frequency of 3 GHz can couple to this 2nd-order exceptional point, and the evolution of the wave is shown in Fig. 7. It can be seen from the figure that the initially propagating surface wave gets instantaneously amplified when the PSTC is turned on. The amplified surface wave continues propagating in the same direction, and an amplified surface wave is also backward radiated in the opposite direction. The PSTC here behaves as an antenna radiating waves.

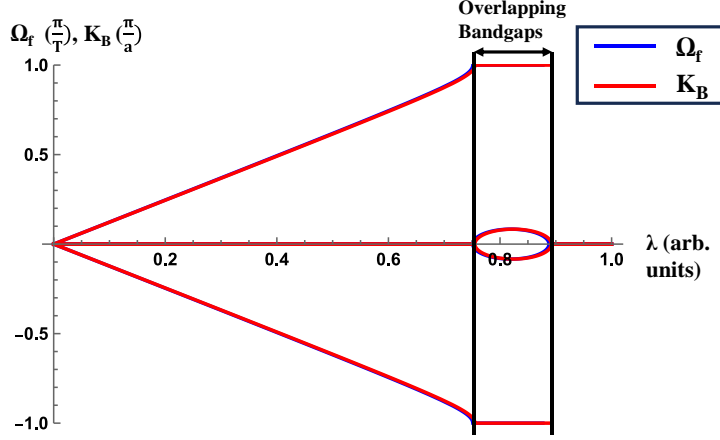


Fig. 6. Dispersion relation of a 2D PSTC showing perfect overlap of the energy and momentum bandgaps.

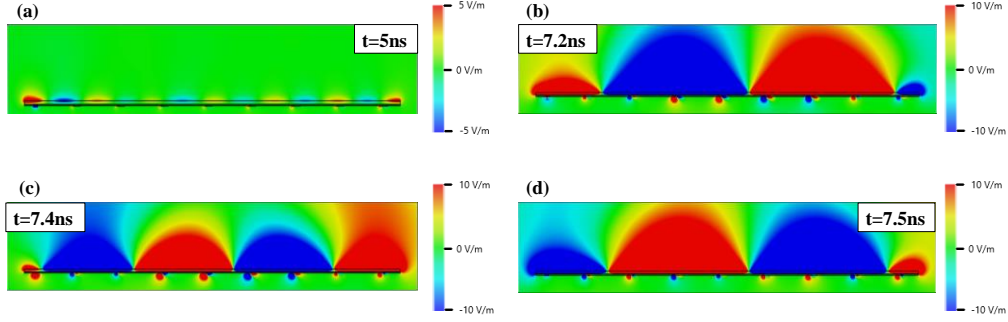
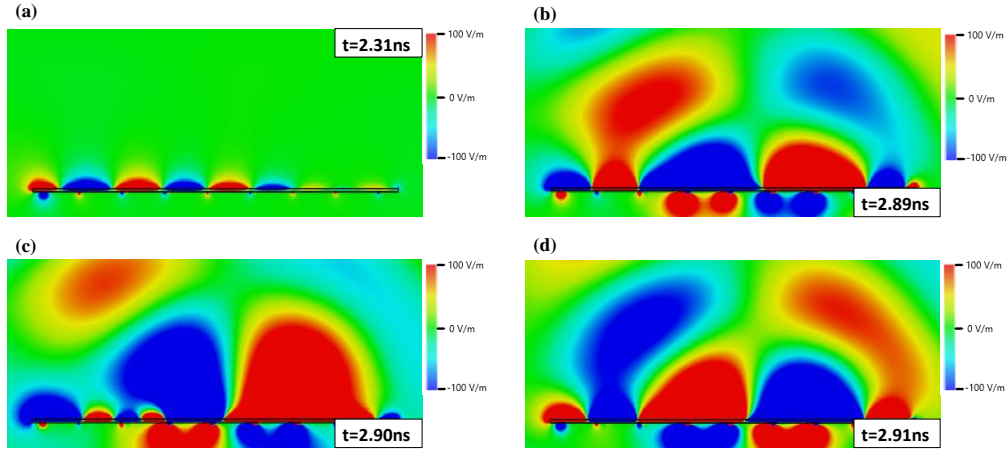


Fig. 7. (a) TE surface wave before the PSTC is turned on at  $t = 5$  ns. The lobes of  $\vec{E}_y$  can barely be seen in Figure (a) because it has a low amplitude. (b), (c), and (d) Wave evolution of TE surface wave after the PSTC is turned on at  $t = 5$  ns.

## 6. Possibility of making a surface antenna for 6G wireless communications using 2D PSTC

Our proposed metasurface-based 2D PSTC can be used as a surface antenna [27], capable of working with both surface and free-space waves, as demonstrated in Supplemental 1 (S4). Here, we have shown that by modifying the metasurface used in all other simulations, a metasurface-based PSTC can be designed to operate at the high frequencies used in 6G communications. We replaced the lossy FR-4 dielectric, used in the original metasurface structure, with a lossy aluminum nitride dielectric, which has a lower loss tangent ( $\tan \delta$ ) value of 0.0003, permittivity ( $\epsilon$ ) = 8.6 F/m, and permeability ( $\mu$ ) = 1 H/m. Additionally, we scaled down the metasurface structure by a factor of 0.067 to make it suitable for practical applications and conducted S-parameter simulations of the modified PSTC structure. The results of these simulations are presented in Supplemental 1 (S5). The S-parameter results shown in Supplemental 1 (S5) indicate that the modified metasurface structure using lossy aluminum nitride as the dielectric allows TE surface waves to propagate along the metasurface or free-space waves to couple surface wave propagating modes having frequencies in the frequency range between 25GHz to 30GHz. These TE surface waves can excite all the eigenmodes of our 2D photonic space-time crystal. The transmission coefficient is maximum in the frequency range of 25GHz to 30GHz.

Thus, we can utilize this scaled-down metasurface-based PSTC with lossy aluminum nitride dielectric as a 5G and 6G surface antenna for wireless communications, as this frequency range corresponds to the 5G high-band and 6G upper mid-band frequencies. To validate this, we conducted FDTD simulations of a TE surface wave with a frequency of 25GHz propagating along the metasurface. At this frequency, the transmission coefficient is maximum, as shown in the S-parameter results. We found that with a crystal having a modulation frequency of 28GHz and a spatial period of 10.7mm, the TE surface wave at 25GHz frequency can excite an exceptional point mode. The wave evolution is depicted in Fig. 8. When the PSTC is activated at  $t = 2.5\text{ns}$ , the TE wave ceases propagation, and its amplitude is instantaneously amplified. The amplified surface wave continues propagating in its original direction, while an amplified surface wave is also radiated in the opposite direction. The metasurface also radiates into free space, as shown in Fig. 8. Hence, the metasurface-based PSTC serves as an antenna radiating waves, as illustrated in Fig. 8(b), Fig. 8(c), and Fig. 8(d). See Supplemental 1 (S5) for more information on the antenna.



**Fig. 8.** (a) TE surface wave propagating along the metasurface before the PSTC is turned on at  $t = 2.5\text{ns}$ . (b), (c), and (d) TE surface wave couples to an exceptional point eigenmode and the surface wave stops propagating, the surface wave's amplitude rapidly amplifies and the amplified surface wave keeps on propagating along the initial direction and an amplified surface wave is also radiated in the opposite direction. Free space radiation also happens as can be seen in (b), (c), and (d).

## 7. Conclusion

In conclusion, this paper proposes, designs, and simulates for the first time a metasurface-based photonic space-time crystal (PSTC), a 2D surface where surface capacitance varies simultaneously with time and space. We calculate and plot the dispersion relation of the 2D PSTC. We demonstrate the characteristic behavior of different eigenmodes corresponding to various types of bandgaps in the dispersion relation. The paper showcases the characteristic behavior of mixed energy-momentum bandgap eigenmodes of the 2D PSTC, resulting from the partial overlap of energy and momentum bandgaps in the band structure. Additionally, the paper demonstrates the wave evolution of exceptional point eigenmodes that arise when energy and momentum bandgaps completely overlap in the dispersion relation of the 2D PSTC. Furthermore, we show that all eigenmodes of our proposed metasurface-based PSTC can be excited by free-space TE waves, making it suitable for use as a surface antenna. We practically realize a PSTC working not only in the radio frequency domain but also in 5G high-band and

6G upper mid-band frequency ranges. By changing the substrate of the metasurface and scaling down its structure, we verify in this article that our metasurface-based PSTC can be utilized for 5G/6G wireless communications. The practical realization of photonic space-time crystals (PSTC) using metasurfaces, demonstrated in this paper, will aid researchers in exploring PSTCs and advancing their understanding of PSTCs.

**Funding.** M. R. C. Mahdy acknowledges the support of the internal CTGRC grant 2023-24 of North South University (approved by the members of BOT), Bangladesh.

**Disclosures.** The authors declare no conflicts of interest.

**Data availability.** Data underlying the results in this paper are not publicly available at this time but may be obtained from the authors upon reasonable request.

**Supplemental document.** See Supplement 1 for supporting content.

## References

1. F. R. Morgenthaler, "Velocity modulation of electromagnetic waves," *IRE Trans. Microw. Theory Tech.* 6, 167–172 (1958).
2. D. Holberg and K. Kunz, "Parametric properties of fields in a slab of time-varying permittivity," *IEEE Trans. Antennas Propag.* 14, 183–194 (1966).
3. J. T. Mendonça, A. Guerreiro, and A. M. Martins, "Quantum theory of time refraction," *Phys. Rev. A* 62, 033805 (2000).
4. A. B. Shvartsburg, "Optics of nonstationary media," *Phys. Usp.* 48, 797 (2005).
5. F. Biancalana, A. Amann, A. V. Uskov, et al., "Dynamics of light propagation in spatiotemporal dielectric structures," *Phys. Rev. E* 75, 046607 (2007).
6. J. T. Mendonça and P. K. Shukla, "Time refraction and time reflection: two basic concepts," *Phys. Scripta* 65, 160 (2002).
7. J. R. Zurita-Sánchez, J. H. Abundis-Patiño, and P. Halevi, "Pulse propagation through a slab with time-periodic dielectric function  $\epsilon(t)$ ," *Opt. Express* 20, 5586–5600 (2012).
8. J. R. Reyes-Ayona and P. Halevi, "Observation of genuine wave vector ( $k$  or  $\beta$ ) gap in a dynamic transmission line and temporal photonic crystals," *Appl. Phys. Lett.* 107, 074101 (2015).
9. A. M. Shaltout, J. Fang, A. V. Kildishev, et al., "Photonic time-crystals and momentum band-gaps," in *Conf. Lasers Electro-Optics* (2016).
10. E. Lustig, Y. Sharabi, and M. Segev, "Topological aspects of photonic time crystals," *Optica* 5, 1390–1395 (2018).
11. N. Wang, Z.-Q. Zhang, and C. T. Chan, "Photonic Floquet media with a complex time-periodic permittivity," *Phys. Rev. B* 98, 085142 (2018).
12. V. Pacheco-Peña and N. Engheta, "Temporal aiming," *Light Sci. Appl.* 9, 129 (2020).
13. Y. Sharabi, E. Lustig, and M. Segev, "Disordered photonic time crystals," *Phys. Rev. Lett.* 126, 163902 (2021).
14. G. Castaldi, V. Pacheco-Peña, M. Moccia, et al., "Exploiting space-time duality in the synthesis of impedance transformers via temporal metamaterials," *Nanophotonics* 10, 3687–3699 (2021).
15. F. Ding, A. Pors, S. I. Bozhevolnyi, et al., "Spatiotemporal isotropic-to-anisotropic meta-atoms," *New J. Phys.* 23, 095006 (2021).
16. H. Li, S. Yin, E. Galiffi, et al., "Temporal parity-time symmetry for extreme energy transformations," *Phys. Rev. Lett.* 127, 153903 (2021).
17. D. Ramaccia, A. Alu, A. Toscano, et al., "Propagation and scattering effects in metastructures based on temporal metamaterials," in *15th Int. Congr. Artif. Mater. Nov. Wave Phenomena, Metamaterials* (2021), pp. 356–358.
18. R. Maas, J. Parsons, N. Engheta, et al., "Experimental realization of an epsilon-near-zero metamaterial at visible wavelengths," *Nat. Photonics* 7, 907–912 (2013).
19. L. Caspani, R. P. M. Kaipurath, M. Clerici, et al., "Enhanced nonlinear refractive index in  $\epsilon$ -near-zero materials," *Phys. Rev. Lett.* 116, 233901 (2016).
20. D. M. Solis and N. Engheta, "A theoretical explanation for enhanced nonlinear response in epsilon-near-zero media," in *CLEO* (2020).
21. Y. Zhou, M. Z. Alam, M. Karimi, et al., "Broadband frequency translation through time refraction in an epsilon-near-zero material," *Nat. Commun.* 11, 2180 (2020).
22. V. Bruno, C. Devault, S. Vezzoli, et al., "Negative refraction in time-varying strongly coupled plasmonic-antenna-epsilon-near-zero systems," *Phys. Rev. Lett.* 124, 043902 (2020).
23. V. Bruno, S. Vezzoli, C. De Vault, et al., "Broad frequency shift of parametric processes in epsilon-near-zero time-varying media," *Appl. Sci.* 10, 1318 (2020).

24. Taravati, Sajjad, and George V. Eleftheriades. "Pure and linear frequency-conversion temporal metasurface." *Physical Review Applied* 15.6 (2021): 064011.
25. Taravati, Sajjad, and George V. Eleftheriades. "Microwave space-time-modulated metasurfaces." *ACS Photonics* 9.2 (2022): 305-318.
26. R. El-Ganainy, K. G. Makris, D. N. Christodoulides, et al., "Theory of coupled optical PT-symmetric structures," *Opt. Lett.* 32, 2632–2634 (2007).
27. A. Shojaeifard, K.-K. Wong, K.-F. Tong, et al., "Mimo evolution beyond 5g through reconfigurable intelligent surfaces and fluid antenna systems," *Proc. IEEE* 110, 1244–1265 (2022).